CrystEngComm

PAPER

View Article Online
View Journal | View Issue

Check for updates

Cite this: *CrystEngComm*, 2017, **19**, 6116

# Capture of volatile iodine by newly prepared and characterized non-porous $[CuI]_n$-based coordination polymers†

Abbas Tarassoli,*[a] Valiollah Nobakht,*[a] Elham Baladi,[a] Lucia Carlucci[b] and Davide M. Proserpio[bc]

Received 27th June 2017,
Accepted 11th September 2017

DOI: 10.1039/c7ce01193h

rsc.li/crystengcomm

Four new non-porous CuI-coordination polymers $[Cu_2(\mu_3\text{-}I)_2(\mu\text{-bpb})]_n$ (**1a**), $[Cu(\mu_2\text{-}I)(\mu\text{-bpb})]_n$ (**1b**), $[Cu_4(\mu_2\text{-}I)_4(\mu\text{-bpmb})_4]_n$ (**2**), and $[CuI(\mu\text{-bdb})]_n$ (**3**) (bpb = 1,4-bis(pyrazolyl)butane; bpmb = 1,4-bis[(pyrazolyl)methyl]benzene; bdb = 1,4-bis[(3,5-dimethylpyrazolyl)methyl]benzene) have been successfully prepared and their structures fully characterized by single-crystal X-ray diffraction, FT-IR spectroscopy, PXRD and elemental analysis. Crystallographic investigation revealed that **1a**, **1b**, and **2** exhibit two-dimensional (2D) structures; in **1a** parallel $[Cu_2I_2]_n$ staircase motifs are cross-linked into two-dimensional sheets by bpb linkers with a fully extended conformation, while in the structures of **1b** and **2** $Cu_2I_2$ rhomboid dimers are linked by bpb and pbmb ligands, respectively, into two-dimensional sheets with a $4^4$-**sql** net. Differently, compound **3** shows a one-dimensional (1D) zigzag chain structure with monomeric CuI units. All the four non-porous coordination polymers show the ability to capture volatile iodine in the gas phase. The solid-state photoluminescence properties of **1a**, **1b**, and **2** have also been investigated. The iodine-adsorbed samples **1a**-$I_2$, **1b**-$I_2$, and **2**-$I_2$ show no fluorescence behavior.

## Introduction

Coordination polymers (CPs) and metal–organic frameworks (MOFs) are interesting categories of materials consisting of metal ions or metal clusters connected by organic linker ligands.[1] Various metal clusters, especially metal carboxylate aggregates, have been used as secondary building units (SBUs) in the self-assembly of CPs and MOFs.[2] Copper(I) iodides are also building blocks in the synthesis of metal–organic materials.[3] Intense investigation in the past three decades in this area of research was conducted not only because of the structural diversity of copper iodide based polymers but also because of the uniqueness of the luminescence properties of the copper(I) iodide aggregates.[4] Reactions of copper(I) iodide with nitrogen or sulfur donor linkers in some organic solvents convert the 3D structure of bulk CuI into zero-dimensional $Cu_nI_n$ ($n$ = 2–12) aggregates or into various one- to three-dimensional motifs which also have different physical and chemical properties. The structural diversity and synthetic routes of copper(I) halide aggregates have been reviewed by R. Peng *et al.* in detail.[3] On the other hand, it should be remembered that the world energy consumption will greatly increase in the near future and nuclear power plants are important energy sources to produce electricity on a large scale. However, the production of radioactive waste and appropriate disposal of such nuclear materials are still unsolved problems.[5] Nuclear wastes contain radioisotopes with long half-lives. This means that the radioisotopes stay in the atmosphere and are hazardous to health for thousands of years. Radioactive iodine isotopes, $^{133}I_2$, $^{131}I_2$, $^{129}I_2$, $^{125}I_2$, are the main components of nuclear wastes. These are volatile hazardous species and are involved in human metabolic processes.[6] Among them, radioisotope $^{129}I_2$ remains in the environment for a long time due to its half-life of 15.7 million years. Due to the harmful effects of radioactive iodine on human health, a safe capture process and subsequent long-term storage by effective adsorbents is extremely important. To find a suitable matrix for capturing radioactive iodine, several different types of adsorbents such as silver-containing zeolite mordenite,[7] Hofmann clathrates,[8] layered double hydroxides (LDHs),[9] porous carbon,[10] porous organic frameworks[11] and metal–organic frameworks (MOFs)[12,13] have already been reported so far. The silver-containing zeolite (AgZ) mordenite has been a benchmark of iodine capture for many years.

[a] *Department of Chemistry, Faculty of Sciences, Shahid Chamran University of Ahvaz, Ahvaz, Iran. E-mail: tarassoli@scu.ac.ir, v.nobakht@scu.ac.ir; Fax: +98 613 3331042*
[b] *Dipartimento di Chimica, Università degli Studi di Milano, Via C. Golgi 19, 20133, Milano, Italy*
[c] *Samara Center for Theoretical Materials Science (SCTMS), Samara University, Samara 443011, Russia*

† Electronic supplementary information (ESI) available. CCDC 1556162–1556165. For ESI and crystallographic data in CIF or other electronic format see DOI: 10.1039/c7ce01193h

Open Access Article. Published on 11 September 2017. Downloaded on 4/20/2024 12:18:07 AM.
This article is licensed under a Creative Commons Attribution-NonCommercial 3.0 Unported Licence.


This journal is © The Royal Society of Chemistry 2017

Open Access Article. Published on 11 September 2017. Downloaded on 4/20/2024 12:18:07 AM.
This article is licensed under a Creative Commons Attribution-NonCommercial 3.0 Unported Licence.

However, iodine diffusion inside the zeolite is slow and limits the capture efficiency. On the other hand, the sorbent requires silver to bind $I_2$(g) and hence the preparation of AgZ is expensive.[14] In particular, MOFs exhibit high iodine sorption efficiency due to their higher porosity compared to zeolite-like materials.[13] Various MOFs containing different nodes and linkers have been reported and their tendency to absorb iodine molecules in the vapor or liquid phase has been examined.[12] Among the various adsorbent materials, MOFs seem to be one of the most effective candidates for the capture of iodine. Sorption of iodine by MOFs may occur physically or chemically, known as physisorption and chemisorption, respectively. In physisorption, iodine molecules usually diffuse and encapsulate into the channels or voids of porous MOFs, whereas in the chemisorption process, a chemical interaction or chemical reaction occurs between the $I_2$ molecules and the MOF surface. Although distinguishing between chemisorption and physisorption is not simple, Kawano and co-workers clearly visualized physi- and chemisorption of iodine in $Cu_2I_2$-based porous MOFs by single crystal X-ray diffraction.[12c] Crystal-structure analysis confirms the chemisorption of iodine molecules through the formation of an $I_3^-$ group from each bridging iodide unit with an almost linear geometry for the $I_3^-$ ion. Thus, $Cu_nI_n$ moieties in copper iodide-based metal–organic materials may be versatile groups for the capture of volatile iodine, even by non-porous CPs in the gas phase. With this idea in mind and as a continuation of our previous work on the synthesis of copper(I) based CPs,[15] we have prepared four non-porous coordination polymers with flexible bidentate linker ligands (Scheme 1) and investigated their ability to capture volatile iodine in the gas phase. The photoluminescence behavior of the complexes **1a**, **1b**, and **2** and its relation with iodine capture was also investigated.

## Results and discussion

### Description of crystal structures

**Crystal structure of $[Cu_2(\mu_3\text{-}I)_2(\mu\text{-bpb})]_n$ (1a).** Single-crystal X-ray diffraction at 298 K reveals that **1a** crystallizes in the monoclinic $P2_1/c$ space group with $Z$ = 2. **1a** is a 2D sheet structure composed of 1D $[Cu_2I_2]_n$ inorganic ladders and μ-bpb organic linkers. The asymmetric unit consists of one copper(I), one iodo, and half of a bpb linker (Fig. 1a). There is a crystallographic inversion center at the mid-point of the $-(CH_2)_4-$ spacer group of the bpb ligand. The Cu(I) ion is coordinated by a bbd N atom with a Cu–N distance of 2.032(4) Å and three triply bridging symmetry-related iodide anions with Cu–I distances of 2.6162(10)–2.7343(10) Å in a distorted tetrahedral $CuNI_3$ coordination geometry (Table S1 in the ESI†). The angles around each copper atom, ranging from 103.22(13)° to 121.10(12)°, indicate a smaller deviation from the ideal tetrahedral geometry with respect to that observed in a related structure with the bis methylated bpb $[Cu_2(\mu_3\text{-}I)_2(\mu\text{-}1,4\text{-bis}(3,5\text{-dimethylpyrazol-1-yl})\text{butane})]_n$.[15a] In the latter, the larger deviation [93.03(3)° to 121.77(15)°] may be ascribed to the steric hindrance of the Me substituents on the pyrazolyl rings. In **1a**, two copper ions and two bridging iodines form $Cu_2I_2$ rhomboid units with Cu···Cu distances of 2.92 and 3.20 Å. Each rhomboid ring shares two opposite edges with adjacent rings to give one-dimensional polymeric staircase ladders. The dihedral angle between adjacent $Cu_2I_2$ rings is 117.36°. Parallel 1D $[Cu_2I_2]_n$ ladders are connected together by bridging bpb ligands to form an undulating sheet structure (Fig. 1b and c) with the quite common binodal 3,4-coordinated net **bey** (known as 3,4L83 in ref. 16).

The pyrazolyl rings of the adjacent bpb ligands in a sheet are parallel by symmetry; however the centroid···centroid distance of 4.389 Å implies no significant π···π interaction. The $[Cu_2I_2]_n$ ladders run along the crystallographic $a$ axis and the sheets lie parallel to the $ac$ plane. As indicated in Fig. 1c, parallel sheets interdigitate and pack in an ABAB fashion along the $b$ axis. The stacking of the 2D sheets generate weak C–H···I interactions in the range 3.18–3.22 Å.

**Crystal structure of $[Cu(\mu\text{-}I)(\mu\text{-bpb})]_n$ (1b).** Compound **1b** was isolated from the same reaction mixture of **1a**. It crystallizes in the monoclinic $P2_1/n$ space group with $Z$ = 4 as a 2D structure composed of rhomboid $Cu_2I_2$ inorganic nodes and μ-bpb organic linkers. The asymmetric unit of **1b** contains one copper(I) ion, one iodo and a bpb ligand (Fig. 2a). The $Cu_2I_2$ rhomboid dimers are connected to four other dimers by bridging bpb ligands. The Cu···Cu distance in the $Cu_2I_2$ units is 2.8036(5) Å, comparable with the sum of the van der Waals radii of copper(I) (2.80 Å),[17] implying weak Cu···Cu bonding interactions. The Cu–I bonds in the $Cu_2I_2$ planar 4-ring show a slight deviation from the ideal rhombic geometry with distances in the range 2.6940(4)–2.7140(5) Å, comparable with the values observed in coordination polymers with $Cu_2I_2$ cores.[18] Each copper atom is coordinated by two N atoms from bpb linkers and two $\mu_2$-I ions, giving a $CuN_2I_2$ moiety with bond angles ranging from 100.92(6)° to 124.19(9)° (Table S1 in the ESI†). Remarkable deviations from the ideal tetrahedral geometry can be due to the presence of two bulky pyrazolyl rings on the organic ligand and the iodine atoms around the metal center, deviations that can be evaluated by the $\tau_4$ value, introduced by Houser *et al.*[19] to

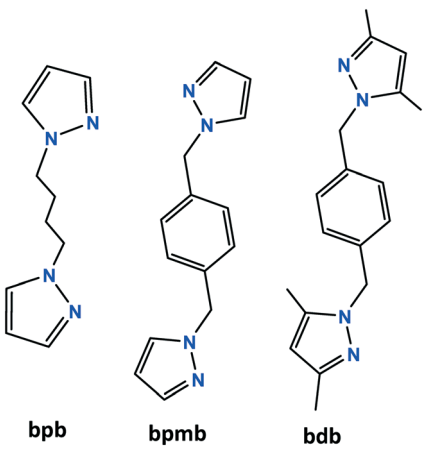


Scheme 1 Structure of the ligands used in this work.

Open Access Article. Published on 11 September 2017. Downloaded on 4/20/2024 12:18:07 AM.
This article is licensed under a Creative Commons Attribution-NonCommercial 3.0 Unported Licence.

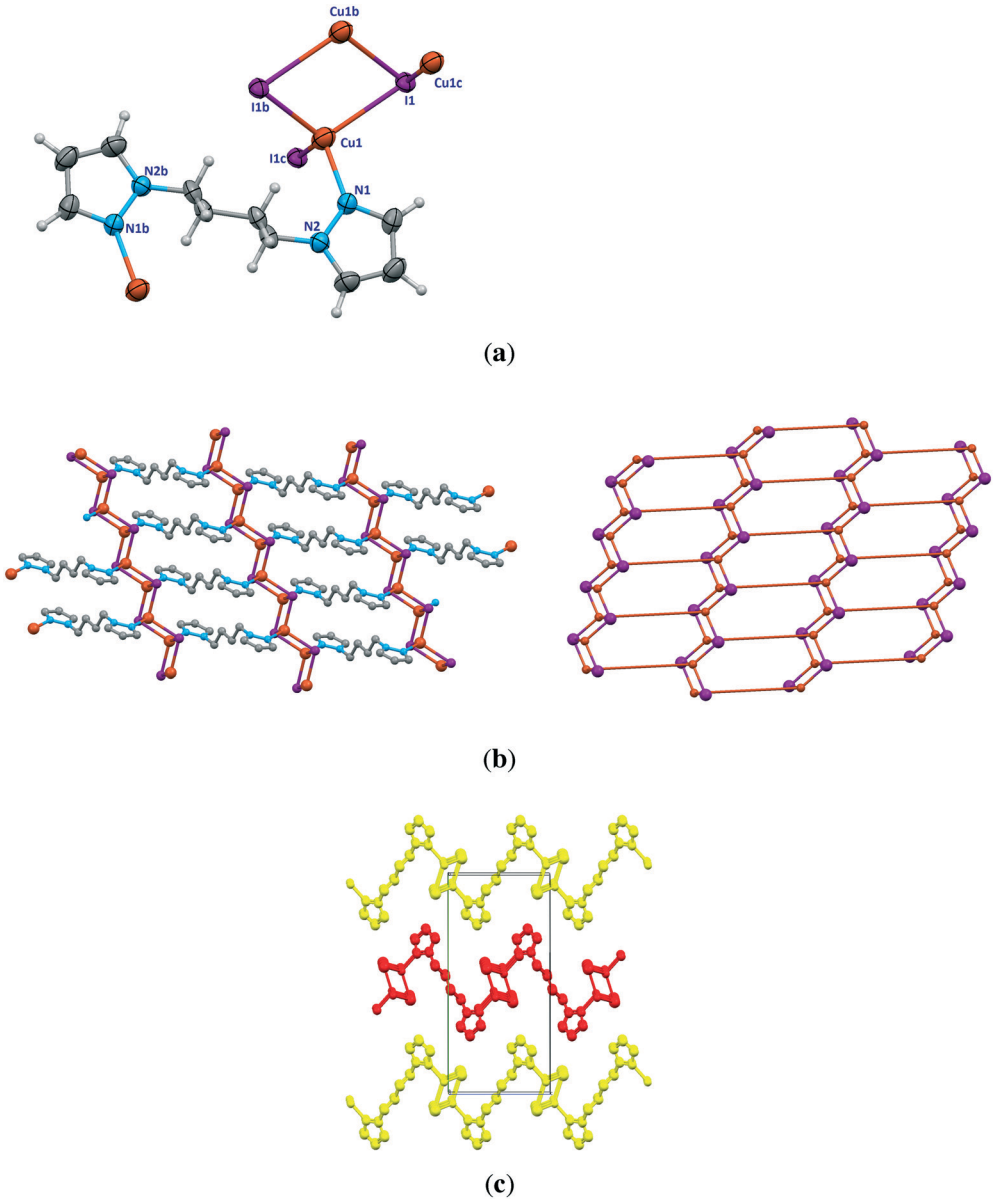


**Fig. 1** The structure of $[Cu_2(\mu_3\text{-}I)_2(\mu\text{-bpb})]_n$ (**1a**). (a) Asymmetric unit of **1a** with additional atoms to complete the bpb ligand and the coordination of Cu and I. (b) 2D polymeric structure with parallel staircase $[Cu_2I_2]_n$ units and the underlying net **bey**. (c) View of the ABAB packing modes of three parallel undulating sheets along the [1 0 0] direction.

describe the geometry of a four-coordinate metal center. The values of $\tau_4$ range from 1.00 for a perfect tetrahedral geometry to zero for a perfect square planar geometry. The calculated $\tau_4$ value of 0.839 for copper ions in **1b** assigns the geometry to a distorted trigonal pyramidal geometry (with the ideal value of 0.85). The bpb molecules act as a bidentate bridging ligand coordinating $Cu_2I_2$ dimers through its nitrogen atoms to form a polymeric two-dimensional structure with a $4^4$-**sql** topology (Fig. 2b) with the dimers as 4-c nodes. $Cu_2I_2$ nodes and bpb linkers form a rhombic window with an edge of 10.77 Å (distance between the centroids of $Cu_2I_2$) and the two diagonals of 19.42 and 9.34 Å (Fig. 2b). The layers stack along the [0 0 1] direction in an AAA mode with a distance of 7.11 Å between the average planes of adjacent layers. All the $\mu_2$-bpb ligands are crystallographically equivalent and exhibit an *anti–anti–anti* conformation for the $-(CH_2)_4-$ spacer with a (Cu)N-to-N(Cu) distance of 7.80 Å. The ligand length in **1b** is comparable with those reported for the related 1,4-bis[3,5-dimethylpyrazol-1-yl]butane (bbd) ligand with the same butyl spacer in $[WS_4Cu_2(\mu\text{-bbd})]_n$,[20] $[Cu_2(\mu_3\text{-Br})_2(\mu\text{-bbd})]_n$,[15a] and $[(WS_4Cu_3I)_2(\mu\text{-bbd})_3]_n{\cdot}n$(DMF).[15b] However, the distance (0.73–1.47 Å) is remarkably larger than the ones reported for $[Zn(NCS)_2(\mu\text{-bbd})]_n$, $[ZnI_2(\mu\text{-bbd})]_n$,[21] and $[WS_4Cu_5I_3(\mu\text{-bbd})_2]_n$.[15b] The difference in the linker lengths in this type of polymer depends on the sequence of the conformations along the aliphatic butyl chain. A wider separation is achieved when all the four C–C bonds of the $-(CH_2)_4-$ linker between the pyrazolyl rings exhibit an *anti* conformation and

 This journal is © The Royal Society of Chemistry 2017

Open Access Article. Published on 11 September 2017. Downloaded on 4/20/2024 12:18:07 AM.
This article is licensed under a Creative Commons Attribution-NonCommercial 3.0 Unported Licence.

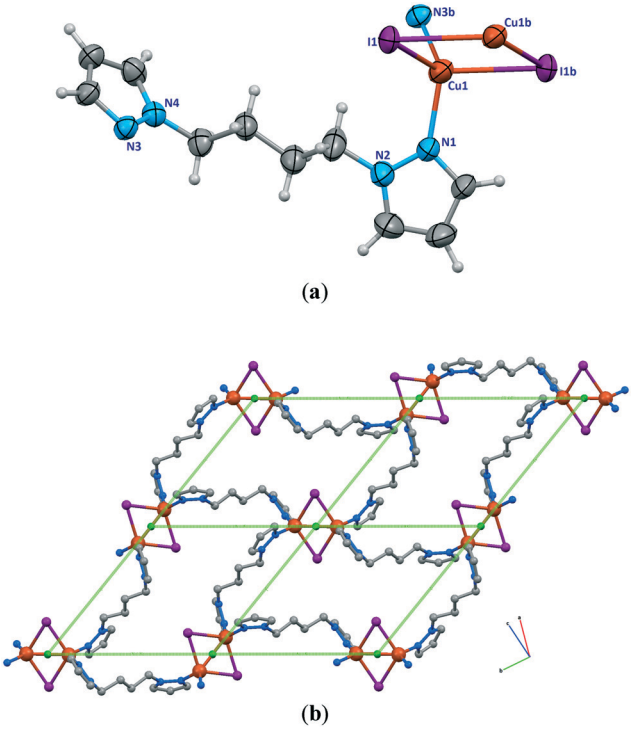


Fig. 2 The structure of [Cu($\mu_2$-I)($\mu$-bpb)]$_n$ (**1b**). (a) Asymmetric unit of **1b** with additional atoms to complete the coordination of Cu. (b) Part of the two-dimensional **4$^4$-sql** net structure with four equal parallelograms.

the pyrazolyl rings choose a dihedral angle of 180°. Hence, *gauche–anti–anti* and *gauche–anti–gauche* conformations provide shorter N-to-N distances for the linkers with respect to the *anti–anti–anti* one.

**Crystal structure of [Cu$_4$($\mu_2$-I)$_4$($\mu$-bpmb)$_4$]$_n$ (2).** Coordination polymer **2** crystallizes in the monoclinic *P*21/*c* space group with the asymmetric unit containing two rhomboid [Cu$_2$I$_2$] dimers and four discrete bpmb ligands (Fig. 3a). The two rhomboid dimers show various Cu–I bond distances, ranging from 2.63 to 2.76 Å, implying a larger deviation from the ideal rhombic geometry compared to analogue dimers in the structure of **1b**. These different Cu–I bond lengths give two different Cu⋯Cu distances, 2.7691(11) and 2.8782(11) Å, in **2**. All the copper atoms have a CuN$_2$I$_2$ coordination environment occupied by two bridging $\mu_2$-iodide and two nitrogen atoms of different bpmb ligands. The bond angles around the Cu1 to Cu4 centers are in the range 100.7–119.8° (Table S1†). The remarkable deviations from the ideal tetrahedral geometry can be explained by the need to accommodate the pyrazolyl rings and the iodine atoms around the copper centers. The calculated $\tau_4$ values for the copper atoms [(Cu1) = 0.891, (Cu2) = 0.895, (Cu3) = 0.885 and (Cu4) = 0.866] evidence the intermediate geometry between the tetrahedral and the trigonal bipyramidal. As for **1b**, the dimeric units are linked together by the bpmb ligands to form non-interpenetrated sheets with **4$^4$-sql** topology (Fig. 3b). However, the presence of four crystallographically independent ligands (shown in different colors in Fig. 3b) with different

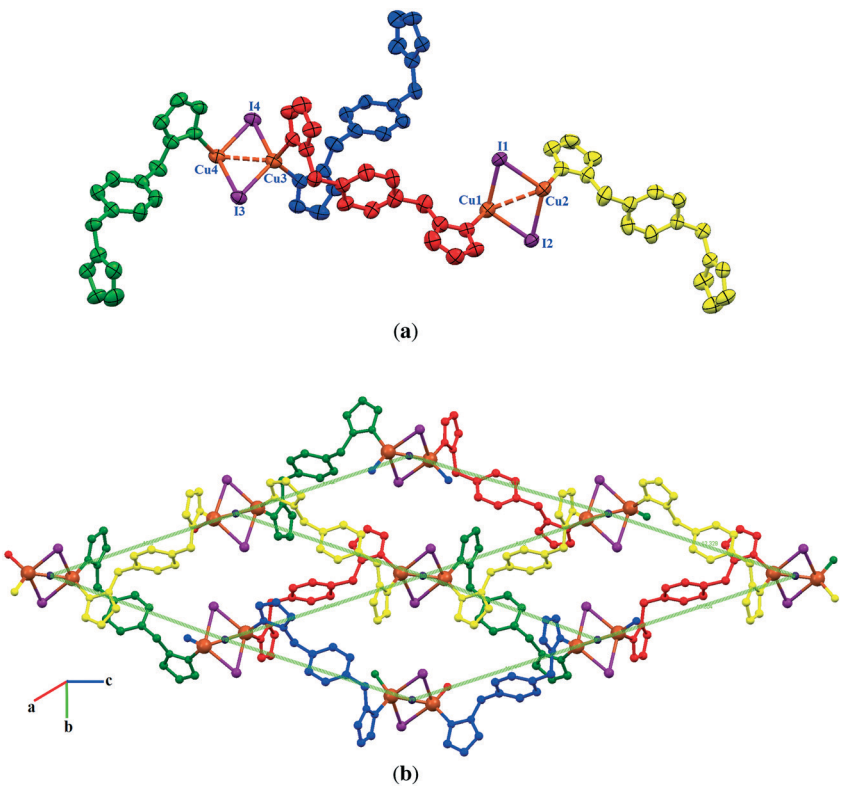


Fig. 3 The structure of [Cu($\mu_2$-I)($\mu$-bpmb)]$_n$ (**2**). (a) Asymmetric unit of **2** with labeling scheme for Cu and I. (b) Part of the two-dimensional structure with four crystallographically independent $\mu$-bpmb linkers shown in different colors.

Open Access Article. Published on 11 September 2017. Downloaded on 4/20/2024 12:18:07 AM.
This article is licensed under a Creative Commons Attribution-NonCommercial 3.0 Unported Licence.

lengths and dihedral angles in the structure of 2 produces two different rhombic windows with unequal lengths [range 11.69–13.02 Å]. This is in contrast to the structure of **1b** where only one type of perfect parallelogram exists. Due to the presence of the –$CH_2$– spacers in the structure of bpmb, two pyrazolyl rings can rotate freely and choose an appropriate position for coordination to the metal centers. Dihedral angles, ligand lengths for the bpmb linkers, and Cu···Cu separations are listed in Table S2.† The red colored ligand shows the more extended structure with a length of 9.39 Å, while the green one displays the shortest distance of 8.97 Å, implying different separations of $Cu_2I_2$ cores in the sheet structure of 2. The dihedral angles between the mean plane of the pyrazolyl and phenyl rings of a ligand are 85.48° and 69.94° (red), 76.54° and 88.67° (yellow), 78.96° and 83.82° (green), and 80.68° and 83.18° (blue).

2D sheets lie parallel to the *bc* plane and show an ABAB packing mode in the crystal. In addition, significant π···π stacking interactions occur in 2. These interactions are of three types, two interlayers (brown and green colored rings) and one intralayer (orange colored rings), with centroid···centroid distances of 3.633(9), 3.594(9), and 3.846(9) Å and dihedral angles of 7.2(9)°, 18.9(8)°, and 18.9(8)°, respectively. These interactions stabilize the structure and link the discrete 2D layers into a 3D network structure (Fig. 4).

**Crystal structure of [CuI(μ-bdb)]$_n$ (3).** Compound 3 is a 1D zigzag chain and crystallizes in the triclinic space group $P\bar{1}$. The asymmetric unit is shown in Fig. 5a. There is a crystallographic inversion center at the midpoint of the phenyl ring of each bdb ligand, so the asymmetric unit consists of one CuI monomer and half each of two bdb ligands. In contrast to the structures of **1a**, **1b**, and 2, compound 3 contains monomeric CuI units. Copper atoms have a trigonal planar coordination geometry with a slight deviation from the ideal geometry and the angles range from 115.18(7)° to 123.53(5)° (Table S1†). The coordination environment of copper atoms is occupied by a terminal I atom with a Cu–I distance of 2.5206(4) Å and two nitrogen atoms of two crystallographically independent bdb ligands with Cu–N distances of 1.9937(18) and 1.9978(17) Å. The N–Cu–I angles [121.29(6)° and 123.52(5)°] are wider than the N–Cu–N one [115.18(8)°]. As expected, the Cu–I bond length in 3 is much shorter than the bridged ones observed for the other compounds. The

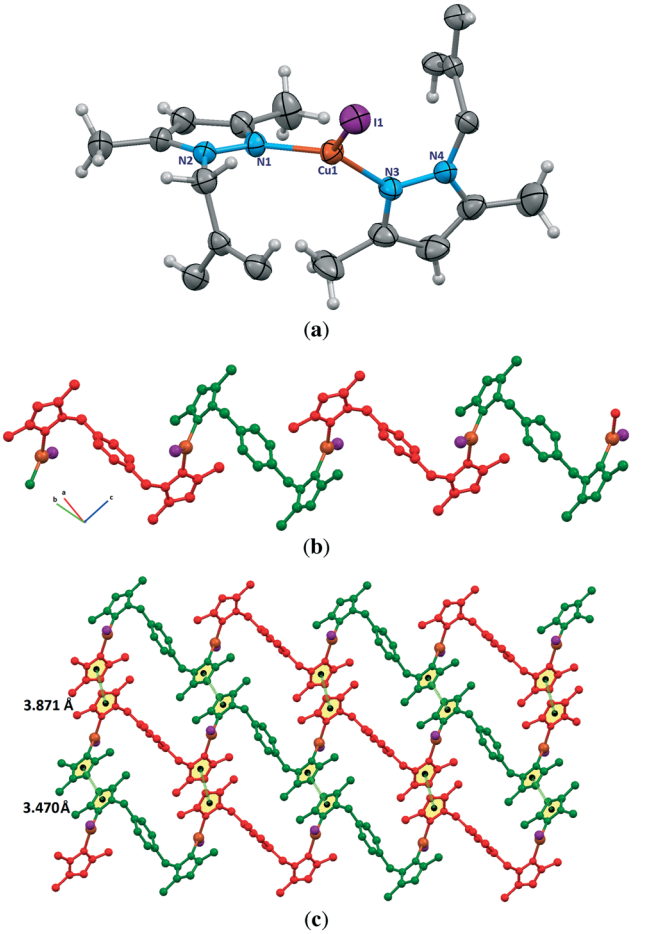


**Fig. 5** The structure of [CuI(μ-bdb)]$_n$ (3). (a) Asymmetric unit of 3 with labeling scheme for non-H and C atoms. (b) 1D zigzag structure of 3 containing a sequence of μ-bdb ligands with two different conformations. (c) π···π stacking interactions between the chains giving 2D supramolecular layers.

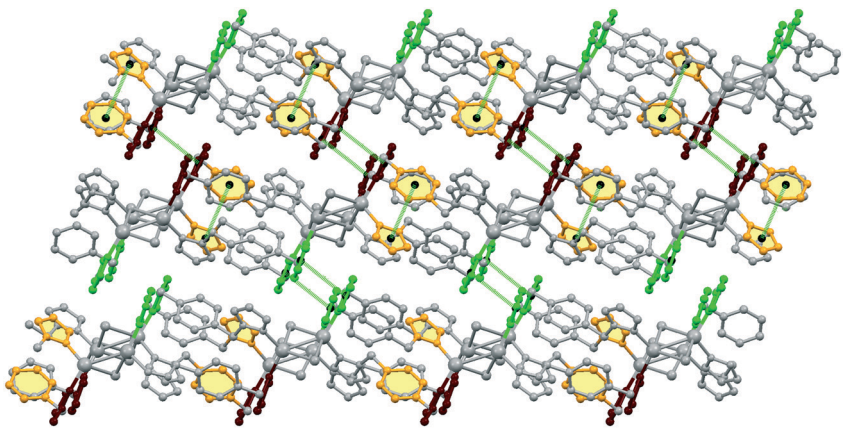

**Fig. 4** Three different π···π stacking interactions in the structure of 2.

 This journal is © The Royal Society of Chemistry 2017

Open Access Article. Published on 11 September 2017. Downloaded on 4/20/2024 12:18:07 AM.
This article is licensed under a Creative Commons Attribution-NonCommercial 3.0 Unported Licence.

structural preference for the trigonal planar arrangement instead of the four-coordinate may be due to the insertion of two methyl substituents on the pyrazolyl rings of bdb, which provide larger steric hindrance around the central copper atoms in **3**. The monomeric CuI units are connected by two independent bdb linkers to form a polymeric one-dimensional zigzag chain running along the [1 1 −1] direction (Fig. 5b). As in the structure of **2** there are crystallographically independent $\mu_2$-bdb ligands in **3**, showing a different pyrazolyl ring rotation around the methylene spacer and consequently different ligand lengths and dihedral and torsion angles. Thus the red colored bdb ligand with a N-to-N distance of 8.73 Å has a greater overall length than the green one (8.20 Å), leading to an alternation of distances between adjacent CuI monomers along the chain, the difference for Cu⋯Cu being close to 0.6 Å (Fig. 5b and c). As both the μ-bdb ligands in the structure of **3** are centrosymmetric, the dihedral angle between two pyrazolyl rings of a ligand are 0° and the nitrogen donor atoms point in exactly opposite directions. This strictly parallel arrangement of rings in the ligands would be better described as antiparallel, with a dihedral angle of 180°. The dihedral angles between the mean plane of the pyrazolyl and phenyl rings of a ligand are 88° (red colored) and 90° (green colored). The 1D zigzag chains pack in a manner such that the pyrazolyl rings of crystallographically equivalent bpb ligands from adjacent chains are strictly parallel and show significant π⋯π interactions. These interactions are of two types with centroid⋯centroid distances of 3.470(2) and 3.871(3) Å and interplanar distances of 3.4141(11) and 3.5787(12) Å between the two rings, respectively. These π⋯π interactions stabilize the structure of **3** and link the discrete 1D chains into a 2D sheet (Fig. 5c).

### Spectroscopic characterization

Infrared spectra of the coordination polymers **1–3** are shown in Fig. S1.† The bands in the range of 3020–3130 $cm^{-1}$ are assigned to the stretching vibration of aromatic C–H bonds of coordinated ligands. Symmetric and asymmetric stretching vibrations of the methylene (–$CH_2$–) and methyl (–$CH_3$) groups of the linkers are observed in the region 2861–2971 $cm^{-1}$. Medium to strong peaks at 1514 (for **1a**), 1517 (for **1b**), 1515 (for **2**) and 1549 (for **3**) $cm^{-1}$ are also observed, which are attributed to the stretching vibration of the C=N bonds of the pyrazolyl rings. In compound **3**, where the pyrazolyl rings bring two methyl substituents, this vibration is shifted to a higher wavenumber with respect to the values found for compounds **1a**, **1b** and **2** containing unsubstituted pyrazolyl rings.

The reproducibility of the syntheses and the phase purity of the products were investigated by powder X-ray diffraction. PXRD patterns are consistent with the structures obtained by single-crystal X-ray diffraction (Fig. 6, S2 and S3†).

### Iodine sorption study

Most of the investigations on iodine sorption have been performed using porous coordination polymers (MOFs) but only in solution.[12b–g] Iodine sorption studies on non-porous coordination polymers in the gas phase are still rare and need to be explored well.[22]

In 2013 Kawano *et al.* reported on the sorption of iodine in the gas phase by a CuI-based 3D porous coordination network, exhibiting crystallographic evidence for the chemisorption of iodine by the $Cu_2I_2$ rhomboid nodes of the structure.[12c] In this case, each Cu–I moiety converts to a Cu–$I_3$ unit without any change in the charge of the network. In addition, recent reports by Zhao *et al.*[12o] and Y.-Z. Zheng *et al.*[12p] also reveal halogen-bond interactions between iodine

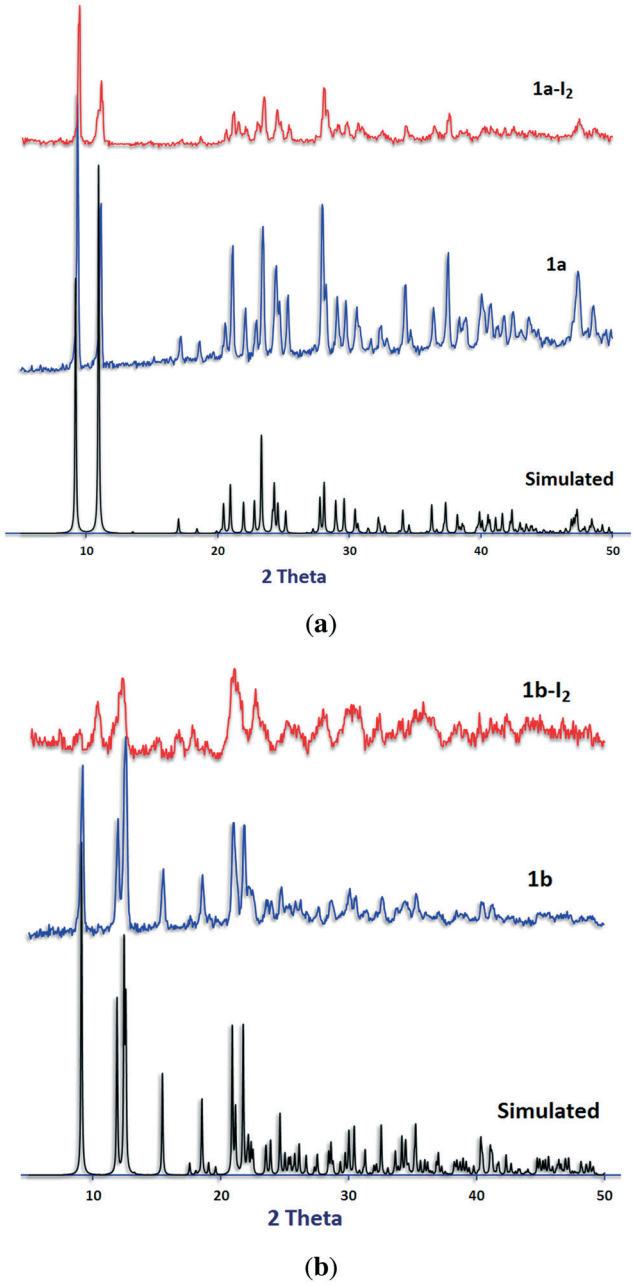


Fig. 6 PXRD patterns for (a) **1a** and (b) **1b**. Calculated from the single-crystal structure (black) before (blue) and after (red) iodine sorption experiments.

Open Access Article. Published on 11 September 2017. Downloaded on 4/20/2024 12:18:07 AM.
This article is licensed under a Creative Commons Attribution-NonCommercial 3.0 Unported Licence.

and the Cu–I moieties present in the structures they studied. On the basis of these results we explored the possibility of iodine capture in the gas phase by the four non-porous $Cu_nI_n$-based coordination polymers **1–3**. Analysis of the structures using the Platon software[23] confirms that there is no accessible void for guest molecules for all.

A fixed iodine vapor pressure strategy was employed, and a vial containing ground colorless crystals of the CPs was kept in a closed system containing crystals of iodine and heated at 55–60 °C at ambient pressure. When the crystals were exposed to iodine vapor, the color of the samples turned to dark brown or black immediately. To evaluate the iodine uptake, the samples were washed with cyclohexane to remove deposited iodine on the surface of the crystals, dried and weighed. Photographs of the samples before and after iodine sorption are shown in Fig. 7. Gravimetric calculations show sorption values of 26.0, 57.0, 57.9, and 92.7 wt% for **1a**, **1b**, **2**, and **3**, respectively.

Iodine uptake in the gas phase degrades the crystallinity of the samples. Several attempts to obtain suitable iodine adsorbed crystals for X-ray crystallography were unsuccessful.

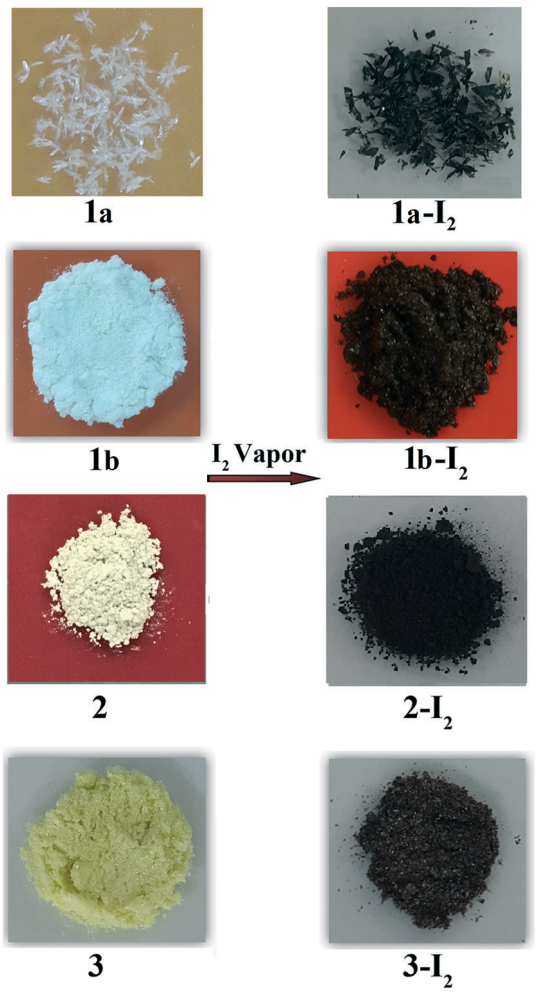


**Fig. 7** Photographs of the samples **1–3** before and after iodine sorption.

Photos of the crystals taken under an optical microscope during gaseous iodine sorption are shown in Fig. S4.†

The FT-IR spectra of compounds **1–3** before and after iodine sorption are almost the same and only the intensity of the vibration bands decreased (Fig. S1†). No other significant difference was observed.

PXRD patterns of the samples after iodine sorption were recorded and are shown in Fig. 6, S2 and S3.† The results show similar PXRD patterns for the iodine-adsorbed samples with respect to their pristine compounds before iodine sorption except for compound **2**.

In order to check the thermal stability of the Cu(I) CPs and to get a better insight into the iodine sorption behavior of the samples, thermal gravimetric analysis (TGA) of **1–3** before and after $I_2$ sorption was performed under a nitrogen atmosphere. As shown in Fig. S5,† all the structures are stable up to about 210 °C and start to collapse at higher temperatures. Comparison between the thermal gravimetric behavior of **1a** and its related iodine-adsorbed **1a**-$I_2$ shows that iodine release occurs at a temperature close to but lower than the decomposition point of **1a**. For compound **1b**-$I_2$, iodine release happens exactly at the decomposition point of **1b**. The results may be a consequence of a strong interaction between iodine molecules and the structures of **1a** and **1b**. The thermal release of the adsorbed iodine from samples **2**-$I_2$ and **3**-$I_2$ occurs at *ca.* 160 °C which is lower than the decomposition point of compounds **2** and **3** (about 240 °C), implying a weaker interaction of iodine molecules with the structures of **2** and **3** with respect to those of **1a** and **1b**. Release of physisorbed iodine from the pores or surface of the MOFs usually occurs at temperatures lower than those of the chemisorbed samples[12b,g,n] due to the weaker interaction between the iodine molecules and the surface of the sorbent at the physisorption process. Hence, the release of iodine molecules at a high temperature of 200 °C, close to the decomposition point of compounds **1a** and **1b**, may be a reason for the chemisorption of iodine. On the other hand, iodine release from the other structures **2** and **3** at lower temperatures may suggest a physisorption process even if the exact interaction mode of iodine with the four structures remains unknown.

To get more insights into the iodine capture process and to confirm the gravimetric iodine uptake amounts in compounds **1–3**, the $I_2$ removal process was also investigated.

Iodine release was investigated in non-polar and polar solvents such as cyclohexane, $CCl_4$, EtOH and DMF. The results show a quick iodine release in DMF, a very slow release in ethanol and $CCl_4$ and no release in cyclohexane. On the contrary, heating the samples under vacuum to release adsorbed iodine was unsuccessful. Results of the iodine release test for **1a** in the four solvents at different times are shown in Fig. S6.† Based on the above results, the iodine content for samples (**1–3**)-$I_2$ were determined by release of the adsorbed iodine in DMF (Fig. S7†) and consequent determination by UV/vis spectroscopy at 368 nm. UV/vis measurements give iodine contents of 23.0, 57.7, 56.6, and 93.8 wt% for **1a**, **1b**, **2**, and

 This journal is © The Royal Society of Chemistry 2017

Open Access Article. Published on 11 September 2017. Downloaded on 4/20/2024 12:18:07 AM.
This article is licensed under a Creative Commons Attribution-NonCommercial 3.0 Unported Licence.

3, respectively (Fig. S8 and Table S3†). These results are consistent with the gravimetric amounts and also comparable to the values reported for porous coordination networks.[12b,c,g]

### Luminescence property

The solid-state photoluminescence properties of **1a**, **1b**, and **2** have been studied at room temperature. The maxima of the emission bands of **1a**, **1b**, and **2** were observed at 556.2, 548.6, and 558.9 nm ($\lambda_{ex}$ = 300 nm), respectively (Fig. 8). The observed photoluminescence could be attributed to MLCT, triplet cluster-centered excited states, a combination of iodine-to-metal charge transfer (IMCT) and d–s transitions by Cu(I)–Cu(I) interaction.[4c,24] An intense yellow emission of **1a** observed visually by the naked eye under UV irradiation (Fig. 8b) is probably due to the presence of staircase $[Cu_2I_2]_n$ SBUs in the structure of **1a**. Interestingly, as iodine species are known as fluorescence quenchers, the fluorescence of the samples is quenched with iodine sorption. The dependence of fluorescence quenching on iodine sorption is an interesting feature observed in this series of CuI-based coordination polymers. This phenomenon has already been observed in a Cd(II)–triazole MOF.[12b] The iodine-release sample **1a**-$I_2$ shows an intense photoluminescence emission again under UV irradiation (Fig. S9†). Such an ON–OFF switching of the photoluminescence emission induced by adsorption/release of iodine in samples **1a**/**1a**-$I_2$ has been shown to be reversible.

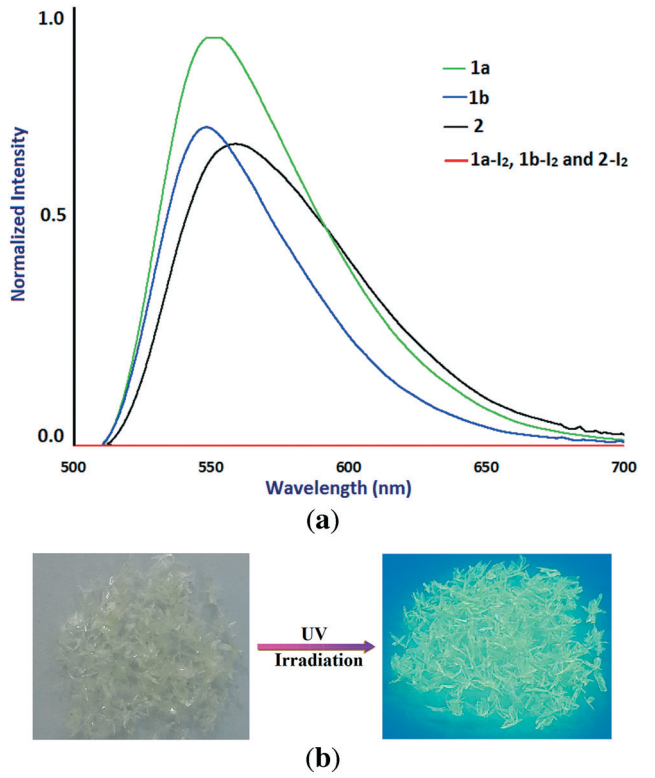


Fig. 8 (a) Solid-state luminescence spectra of **1a** (green), **1b** (blue) and **2** (black) at room temperature ($\lambda_{ex}$ = 300 nm) before and after iodine sorption (red). (b) Crystals of **1a** under UV irradiation at 254 nm at room temperature.

## Experimental

### Materials and physical measurements

All experiments were carried out in air. The starting materials were purchased from commercial sources and used without further purification. Infrared spectra (4000–400 $cm^{-1}$) were recorded as KBr disks on a BOMEN MB102 FT-IR spectrometer. Elemental analyses for C, H and N were performed on a CHNSO Elementar Vario EL III apparatus. X-ray powder diffraction patterns were recorded on a Philips X'Pert Pro diffractometer (Cu Kα radiation, $\lambda$ = 1.54184 Å) in the $2\theta$ range 5–50°. The simulated XRD powder pattern based on single crystal data was prepared using Mercury software.[25] Thermal analyses were carried out on a TGA-DTA Mettler-Toledo TGA/SDTA 851 thermal analyzer between 50 and 600 °C under a dinitrogen atmosphere. Solid-state fluorescence spectra were obtained on a Shimadzu RF-540 spectrofluorometer in the range of 700–500 nm. UV-vis spectra were recorded on a Jenway 6715 spectrophotometer in DMF solution and covered the range 700–200 nm.

### Synthetic procedures

**Preparation of bpb, bpmb, and bdb ligands.** The ligands were prepared according to published methods.[26–29] Typically, a mixture of pyrazole (1.36 g, 20 mmol) or 3,5-dimethyl-1*H*-pyrazole (1.9 g, 20 mmol) and finely powdered potassium hydroxide (2.24 g, 40 mmol) in DMSO (12 mL) was vigorously stirred at 80 °C for 2 h. Then, the corresponding dihalide 1,4-bis(chloromethyl)benzene (1.64 g, 10 mmol) or 1,4-dichlorobutane (1.11 mL, 10 mmol) in DMSO (5 mL) was added dropwise to the slurry mixture. The mixture was stirred at 80 °C until completion of the reaction (checked by TLC). The mixture was cooled to room temperature and the vessel was moved to an ice bath. 250 mL of cooled water was poured into the reaction mixture and a white precipitate formed immediately, which was collected by filtration, washed with water and dried under vacuum. In the case of bpb, as the product is a liquid, the reaction mixture was poured into water (250 mL) and extracted with chloroform (3 × 20 mL). The extract was washed with water (2 × 20 mL) and dried over calcium chloride. After evaporation of chloroform under vacuum, the product was isolated as a yellow oil.

**Preparation of $[Cu_2(\mu_3\text{-}I)_2(\mu\text{-bpb})]_n$ (1a) and $[Cu(\mu_2\text{-}I)(\mu\text{-bpb})]_n$ (1b).** A solution of CuI (0.1 g, 0.52 mmol) in $CH_3CN$ (20 mL) was added to a solution of bpb (0.2 g, 1.04 mmol) in $CH_3CN$ (20 mL) at room temperature; significant amounts of precipitate were formed immediately. The resultant mixture was heated at 100 °C for 6 h. The white precipitate of **1a** was filtered, washed with EtOH and $Et_2O$, and dried in air (**1a**; 0.064 g, 43% yield based on Cu). Colorless rhomboid-shaped crystals of **1b** suitable for X-ray crystallography and a small amount of needle-shaped crystals of **1a** were obtained from the filtrate after five days. They were collected and washed

Open Access Article. Published on 11 September 2017. Downloaded on 4/20/2024 12:18:07 AM.
This article is licensed under a Creative Commons Attribution-NonCommercial 3.0 Unported Licence.

Table 1 Crystallographic data and structure refinement details for **1a–3**

| Compound | 1a | 1b | 2 | 3 |
|---|---|---|---|---|
| Formula | $C_{10}H_{14}Cu_2I_2N_4$ | $C_{10}H_{14}CuIN_4$ | $C_{56}H_{56}Cu_4I_4N_{16}$ | $C_{18}H_{22}CuIN_4$ |
| Molecular weight | 571.13 | 380.69 | 1714.92 | 484.85 |
| $T$ (K) | 296 | 296 | 296 | 296 |
| Cryst syst | Monoclinic | Monoclinic | Monoclinic | Triclinic |
| Space group | $P2_1/c$ | $P2_1/n$ | $P2_1/c$ | $P\bar{1}$ |
| $a$ (Å) | 4.3887(7) | 8.2449(3) | 17.421(7) | 8.8660(12) |
| $b$ (Å) | 19.267(3) | 19.4227(8) | 15.653(6) | 9.0619(12) |
| $c$ (Å) | 8.9217(15) | 8.8011(3) | 23.368(9) | 12.1365(16) |
| $\alpha$ (°) | 90 | 90 | 90 | 91.656(2) |
| $\beta$ (°) | 91.730(3) | 113.635(1) | 105.588(5) | 97.796(2) |
| $\gamma$ (°) | 90 | 90 | 90 | 101.320(2) |
| $V$ (Å$^3$) | 754.0(2) | 1291.17(8) | 6138(4) | 945.7(2) |
| $Z$ | 2 | 4 | 4 | 2 |
| $D_{calcd}$ (g cm$^{-3}$) | 2.515 | 1.958 | 1.856 | 1.703 |
| Data collected | 17 205 | 30 671 | 125 324 | 22 405 |
| Unique data ($R_{int}$) | 2489 (0.037) | 4193 (0.024) | 15 604 (0.050) | 5946 (0.019) |
| Data/restraints/parameters | 2489/0/82 | 4193/0/145 | 15 604/0/721 | 5946/0/221 |
| $R_1$ [$I > 2\sigma(I)$] | 0.0418 | 0.0271 | 0.0313 | 0.0283 |
| w$R_2$ (all data) | 0.0935 | 0.0611 | 0.0715 | 0.0810 |

consecutively with small amounts of EtOH and $Et_2O$ and dried in air (**1b**; 0.063 g, 32% yield based on Cu). Anal. calcd for $C_{10}H_{14}CuIN_4$: C 31.55, H 3.71, N 14.72; found: C 31.35, H 3.58, N 14.87.

*Direct synthesis of **1a**.* A solution of CuI (0.1 g, 0.52 mmol) and $I_2$ (0.13 g, 0.51 mmol) in DMF (10 mL) and a solution of bpb (0.05 g, 0.26 mmol) in DMF (5 mL) were mixed in a Teflon-lined stainless steel autoclave and heated at 120 °C for 24 h. The vessel was gradually cooled to room temperature over 24 h. The yellowish solution was transferred into a Petri dish, and needle-shaped single crystals of **1a** suitable for single crystal X-ray diffraction were obtained after 1 day which were collected by filtration, washed with DMF, EtOH, and $Et_2O$, and dried in air (0.09 g, 63% yield based on Cu).

**Preparation of $[Cu_4(\mu_2\text{-}I)_4(\mu\text{-}bpmb)_4]_n$ (2).** CuI (0.1 g, 0.52 mmol) was added to a solution of bpmb (0.062 g, 0.26 mmol) in DMF (20 mL) and the reaction mixture was stirred overnight at room temperature. The resulting pale yellow solution was filtered. Colorless block-shaped crystals of **2** suitable for X-ray crystallography were obtained at room temperature by slow evaporation of the solvent over two weeks. The crystals were washed with DMF, EtOH, and $Et_2O$ and dried in air (0.09 g, 53% yield based on Cu). Anal. calcd for $C_{56}H_{56}Cu_4I_4N_{16}$: C 39.22, H 3.29, N 13.07; found: C 39.54, H 3.11, N 13.40.

**Preparation of $[CuI(\mu\text{-}bdb)]_n$ (3)**

*Conventional heating.* CuI (0.1 g, 0.52 mmol) was added to a solution of bdb (0.308 g, 1.04 mmol) in DMF (30 mL) and the light green mixture was heated at 90 °C for 6 h. The resulting pale yellow solution was filtered. Pale green crystals of **3** were obtained by leaving the filtrate to stand at room temperature for a week; they were collected and washed consecutively with small amounts of DMF, EtOH, and $Et_2O$, and dried in air (0.23 g, 92.0% yield based on Cu). Anal. calcd for $C_{18}H_{22}CuIN_4$: C 44.59, H 4.57, N 11.56; found: C 44.17, H 4.57, N 11.51.

*Diffusion method.* A solution of CuI (0.01 g) in 3 mL $CH_3CN$ was gently layered on the top of a solution of bdb (0.03 g) in 3 mL $CH_3CN$ in a test tube. Leaf-shaped crystals of **3** suitable for X-ray crystallography were obtained after a week. They were collected and washed with small amounts of $CH_3CN$ and dried in air.

### Iodine sorption study

Certain amounts of **1a–3** crystals (30.0 mg) and solid iodine (*ca.* 30 mg) were added separately to small vials and the vials were placed in a large vessel and sealed. After sublimation of iodine at 55–60 °C, the color of the crystals immediately changed to deep brown or black. To ensure the completion of the process, the samples were exposed to iodine vapor at 55–60 °C for 7 h. The iodine-encapsulated samples were collected, washed with cyclohexane, dried in air, and weighed (37.8, 47.1, 47.4, and 57.8 mg for **1a**-$I_2$, **1b**-$I_2$, **2**-$I_2$, and **3**-$I_2$, respectively).

### Iodine content determination

Iodine-adsorbed **1a**-$I_2$ (9.2 mg), **1b**-$I_2$ (7.2 mg), **2**-$I_2$ (7.8 mg), and **3**-$I_2$ (7.9 mg) samples were added to 5 ml DMF and stirred for 2 min. The resulting orange iodine solutions were filtered and diluted in a 10 ml volumetric flask. The four iodine solutions were diluted to the desired concentration and the corresponding $I_2$ contents were determined by UV/vis spectroscopy at 368 nm.

### Single crystal X-ray crystallographic studies

X-ray data were collected on a Bruker Apex II diffractometer using MoK$\alpha$ radiation. The structures were solved using direct methods and refined using a full-matrix least squares procedure based on $F^2$ using all data.[30] Hydrogen atoms were placed at geometrically estimated positions. Details relating to the crystals and the structural refinements are presented

 This journal is © The Royal Society of Chemistry 2017

Open Access Article. Published on 11 September 2017. Downloaded on 4/20/2024 12:18:07 AM.
This article is licensed under a Creative Commons Attribution-NonCommercial 3.0 Unported Licence.

in Table 1. Full details of crystal data and the structure refinements in CIF format are available as ESI† (CCDC reference numbers 1556162–1556165).

## Conclusion

In summary, four new non-porous copper(I) iodide coordination polymers with diverse bidentate pyrazolyl ligands have been successfully prepared and characterized. The results show that the bispyrazolyl linkers with different spacer groups, lengths, flexibility and steric hindrance on the pyrazolyl rings induce significant effects on the coordination number of copper atoms and dimensionality of the resulting structures. The results confirm that even non-porous CuI coordination polymers show a versatile tendency to capture volatile iodine. Moreover, as the color of the samples immediately turns black when exposed to iodine vapor, these systems could show potential application for iodine sensing purposes. Due to the presence of $[Cu_2I_2]_n$ and $Cu_2I_2$ moieties in the structures of **1a**, **1b**, and **2**, the compounds also show photoluminescence behavior that is quenched with iodine sorption.

## Conflicts of interest

There are no conflicts to declare.

## Acknowledgements

The authors thank Shahid Chamran University of Ahvaz (Grant No. 31400) and the Università degli Studi di Milano (Piano di Sviluppo di Ateneo, azione B, progetti di interesse interdisciplinare PSR2015-1716FDEMA_07) for financial support. DMP acknowledges the Ministry of Education and Science of Russia (Grant 14.B25.31.0005). The authors also thank M. Keshavarzi for designing the graphical abstract.

## References

1 (*a*) H. Furukawa, K. E. Cordova, M. O'Keeffe and O. M. Yaghi, *Science*, 2013, **341**, 974; (*b*) H.-C. Zhou and S. Kitagawa, *Chem. Soc. Rev.*, 2014, **43**, 5415; (*c*) W. Lu, Z. Wei, Z. Gu, T. Liu, J. Park, J. Park, J. Tian, M. Zhang, Q. Zhang, T. Gentle III, M. Bosch and H. Zhou, *Chem. Soc. Rev.*, 2014, **43**, 5561; (*d*) W. L. Leong and J. J. Vittal, *Chem. Rev.*, 2011, **111**, 688.

2 (*a*) V. Guillerm, D. Kim, J. F. Eubank, R. Luebke, X. Liu, K. Adil, M. S. Lah and M. Eddaoudi, *Chem. Soc. Rev.*, 2014, **43**, 6141; (*b*) D. J. Tranchemontagne, J. L. Mendoza-Cortes, M. O'Keeffe and O. M. Yaghi, *Chem. Soc. Rev.*, 2009, **38**, 1257; (*c*) J. J. Perry, J. A. Perman and M. J. Zaworotko, *Chem. Soc. Rev.*, 2009, **38**, 1400.

3 R. Peng, M. Li and D. Li, *Coord. Chem. Rev.*, 2010, **254**, 1.

4 (*a*) G. Zeng, S. Xing, X. Han, B. Xin, Y. Yang, X. Wang, G. Li, Z. Shi and S. Feng, *RSC Adv.*, 2015, **5**, 40792; (*b*) M. Knorr, A. Khatyr, A. D. Aleo, A. E. Yaagoubi, C. Strohmann, M. M. Kubicki, Y. Rousselin, S. M. Aly, D. Fortin, A. Lapprand and P. D. Harvey, *Cryst. Growth Des.*, 2014, **14**, 5373; (*c*) F. Wu, H. Tong, Z. Li, W. Lei, L. Liu, W.-Y. Wong, W.-K. Wong and X. Zhu, *Dalton Trans.*, 2014, **43**, 12463; (*d*) Q. Benito, X. F. L. Goff, G. Nocton, A. Fargues, A. Garcia, A. Berhault, S. Kahlal, J. Saillard, C. Martineau, J. Trebosc, T. Gacoin, J. Boilot and S. Perruchas, *Inorg. Chem.*, 2015, **54**, 4483; (*e*) Q. Benito, X. F. L. Goff, S. Maron, A. Fargues, A. Garcia, C. Martineau, F. Taulelle, S. Kahlal, T. Gacoin, J. Boilot and S. Perruchas, *J. Am. Chem. Soc.*, 2014, **136**, 11311; (*f*) P. M. Graham, R. D. Pike, M. Sabat, R. D. Bailey and W. T. Pennington, *Inorg. Chem.*, 2000, **39**, 5121; (*g*) B. Xin, G. Zeng, L. Gao, Y. Li, S. Xing, J. Hua, G. Li, Z. Shi and S. Feng, *Dalton Trans.*, 2013, **42**, 7562.

5 (*a*) E. Kintisch, *Science*, 2005, **310**, 1406; (*b*) R. C. Ewing and F. N. von Hippel, *Science*, 2009, **325**, 151.

6 (*a*) N. R. Soelberg, T. G. Garn, M. R. Greenlagh, J. D. Law, R. Jubin, D. M. Strachan and P. K. Thallapally, *Sci. Technol. Nucl. Install.*, 2013, **12**, 702496; (*b*) A. Saiz-Lopez, J. M. C. Plane, A. R. Baker, L. J. Carpenter, R. von Glasow, L. C. G. Martin, G. McFiggans and R. W. Saunders, *Chem. Rev.*, 2012, **112**, 1773; (*c*) J. E. T. Hoeve and M. Z. Jacobson, *Energy Environ. Sci.*, 2012, **5**, 8743; (*d*) E. Barea, C. Montoro and J. A. R. Navarro, *Chem. Soc. Rev.*, 2014, **43**, 5419.

7 K. W. Chapman, P. J. Chupas and T. M. Nenoff, *J. Am. Chem. Soc.*, 2010, **132**, 8897.

8 (*a*) G. Massasso, J. Long, J. Haines, S. Devautour-Vinot, G. Maurin, A. Grandjean, B. Onida, B. Donnadieu, J. Larionova, C. Guérin and Y. Guari, *Inorg. Chem.*, 2014, **53**, 4269; (*b*) G. Massasso, M. Rodríguez-Castillo, J. Long, J. Haines, S. Devautour-Vinot, G. Maurin, A. Grandjean, B. Onida, B. Donnadieu, J. Larionova, C. Guérina and Y. Guaria, *Dalton Trans.*, 2015, **44**, 19357; (*c*) G. Massasso, J. Long, C. Guerin, A. Grandjean, B. Onida, Y. Guari, J. Larionova, G. Maurin and S. Devautour-Vinot, *J. Phys. Chem. C*, 2015, **119**, 9395.

9 S. Ma, S. M. Islam, Y. Shim, Q. Gu, P. Wang, H. Li, G. Sun, X. Yang and M. G. Kanatzidis, *Chem. Mater.*, 2014, **26**, 7114.

10 H. Sun, P. La, Z. Zhu, W. Liang, B. Yang and A. Li, *J. Mater. Sci.*, 2015, **50**, 7326.

11 (*a*) C. Pei, T. Ben, S. Xua and S. Qiu, *J. Mater. Chem. A*, 2014, **2**, 7179; (*b*) Y. Zhuojun, Y. Ye, T. Yuyang, Z. Daming and Z. Guangshan, *Angew. Chem., Int. Ed.*, 2015, **54**, 12733.

12 (*a*) D. F. Sava, M. A. Rodriguez, K. W. Chapman, P. J. Chupas, J. A. Greathouse, P. S. Crozier and T. M. Nenoff, *J. Am. Chem. Soc.*, 2011, **133**, 12398; (*b*) Q. K. Liu, J. P. Ma and Y. B. Dong, *Chem. Commun.*, 2011, **47**, 7185; (*c*) H. Kitagawa, H. Ohtsu and M. Kawano, *Angew. Chem., Int. Ed.*, 2013, **52**, 12395; (*d*) V. Safarifard and A. Morsali, *CrystEngComm*, 2014, **16**, 8660; (*e*) L. Hashemi and A. Morsali, *CrystEngComm*, 2014, **16**, 4955; (*f*) S. Parshamoni, S. Sanda, H. S. Jena and S. Konar, *Chem. – Asian J.*, 2015, **10**, 653; (*g*) W. W. He, S. L. Li, G. S. Yang, Y. Q. Lan, Z. M. Su and Q. Fu, *Chem. Commun.*, 2012, **48**, 10001; (*h*) J. Wang, J. Luo, X. Luo, J. Zhao, D. Li, G. Li, Q. Huo and Y. Liu, *Cryst. Growth Des.*, 2015, **15**, 915; (*i*) J. He, J. Duan, H. Shi, J. Huang, J. Huang, L. Yu, M. Zeller, A. D. Hunter and Z. Xu, *Inorg. Chem.*, 2014, **53**, 6837; (*j*) Z. Yin, Q.-Z. Wang and M.-H. Zeng, *J. Am. Chem. Soc.*, 2012, **134**, 4857; (*k*) J. T.

Open Access Article. Published on 11 September 2017. Downloaded on 4/20/2024 12:18:07 AM.
This article is licensed under a Creative Commons Attribution-NonCommercial 3.0 Unported Licence.

Hughes, D. F. Sava, T. M. Nenoff and A. Navrotsky, *J. Am. Chem. Soc.*, 2013, **135**, 16256; (*l*) D. F. Sava, K. W. Chapman, M. A. Rodriguez, J. A. Greathouse, P. S. Crozier, H. Zhao, P. J. Chupas and T. M. Nenoff, *Chem. Mater.*, 2013, **25**, 2591; (*m*) M. Zeng, Q. Wang, Y. Tan, S. Hu, H. Zhao, L. Long and M. Kurmoo, *J. Am. Chem. Soc.*, 2010, **132**, 2561; (*n*) A. K. Chaudhari, S. Mukherjee, S. S. Nagarkar, B. Joarder and S. K. Ghosh, *CrystEngComm*, 2013, **15**, 9465; (*o*) S. S. Zhao, L. Chen, X. Zheng, L. Wang and Z. Xie, *Chem. – Asian J.*, 2017, **12**, 615; (*p*) Y.-Q. Hu, M.-Q. Li, Y. Wang, T. Zhang, P.-Q. Liao, Z. Zheng, X.-M. Chen and Y.-Z. Zheng, *Chem. – Eur. J.*, 2017, **23**, 8409.

13 C. Falaise, C. Volkringer, J. Facqueur, T. Bousquet, L. Gasnotb and T. Loiseaua, *Chem. Commun.*, 2013, **49**, 10320.

14 J. Liu, B. P. McGrail, D. M. Strachan, J. Liu, J. Tian and P. K. Thallapally, *Encyclopedia of Inorganic and Bioinorganic Chemistry*, John Wiley & Sons, Ltd., 2014, p. 1, DOI: 10.1002/9781119951438.eibc2198.

15 (*a*) A. Beheshti, W. Clegg, V. Nobakht and R. W. Harrington, *Polyhedron*, 2014, **81**, 256; (*b*) A. Beheshti, W. Clegg, V. Nobakht and R. W. Harrington, *Cryst. Growth Des.*, 2013, **13**, 1023; (*c*) A. Beheshti, V. Nobakht, L. Carlucci, D. M. Proserpio and C. T. Abrahams, *J. Mol. Struct.*, 2013, **1037**, 236.

16 T. G. Mitina and V. A. Blatov, *Cryst. Growth Des.*, 2013, **13**, 1655.

17 (*a*) A. Bondi, *J. Phys. Chem.*, 1964, **68**, 441; (*b*) I. M. C. van Amsterdam, M. Ubbink, G. W. Canters and M. Huber, *Angew. Chem., Int. Ed.*, 2003, **42**, 62.

18 (*a*) Z.-P. Deng, H.-L. Qi, L.-H. Huo, S. W. Ng, H. Zhao and S. Gao, *Dalton Trans.*, 2010, **39**, 10038; (*b*) D. Braga, F. Grepioni, L. Maini, P. P. Mazzeo and B. Ventura, *New J. Chem.*, 2011, **35**, 339.

19 L. Yang, D. R. Powell and R. P. Houser, *Dalton Trans.*, 2007, 955.

20 A. Beheshti, W. Clegg, S. A. MousaviFard, R. W. Harrington, V. Nobakht and L. Russo, *Inorg. Chim. Acta*, 2011, **376**, 310.

21 V. Nobakht, A. Beheshti, D. M. Proserpio, L. Carlucci and C. T. Abrahams, *Inorg. Chim. Acta*, 2014, **414**, 217.

22 K. Miyao, A. Funabiki, K. Takahashi, T. Mochida and M. Uruichi, *New J. Chem.*, 2014, **38**, 739.

23 A. L. Spek, *J. Appl. Crystallogr.*, 2003, **36**, 7.

24 (*a*) D. Sun, S. Yuan, H. Wang, H. F. Lu, S. Y. Feng and D. F. Sun, *Chem. Commun.*, 2013, **49**, 6152; (*b*) E. Cariati, X. H. Bu and P. C. Ford, *Chem. Mater.*, 2000, **12**, 3385; (*c*) Y. Song, R. Fan, P. Wang, X. Wang, S. Gao, X. Du, Y. Yang and T. Luanb, *J. Mater. Chem. C*, 2015, **3**, 6249.

25 *Mercury 3.0*, Copyright Cambridge Crystallographic Data Centre, 12 Union Road, Cambridge, CB2 1EZ, UK, 2012.

26 Y. J. Huang, Y. L. Song, Y. Chen, H. X. Li, Y. Zhang and J. P. Lang, *Dalton Trans.*, 2009, 1411.

27 J. F. Ma, J. F. Liu, Y. Xing, H. Q. Jia and Y. H. Lin, *J. Chem. Soc., Dalton Trans.*, 2000, 2403.

28 X. Y. Wang, S. Q. Liu, C. Y. Zhang, G. Song, F. Y. Bai, Y. H. Xing and Z. Shi, *Polyhedron*, 2012, **47**, 151.

29 A. S. Potapov, G. A. Domina, A. I. Khlebnikov and V. D. Ogorodnikov, *Eur. J. Org. Chem.*, 2007, 5112.

30 G. M. Sheldrick, *SHELX97-Programs for Crystal Structure Analysis, release 97–2*, Institut fur Anorganische Chemie der Universitat Gottingen, Gottingen, Germany, 1998.

 This journal is © The Royal Society of Chemistry 2017